Internal Energy Build-up in MALDI

Valérie Gabelica[†], Eric Schulz and Michael Karas

Institut für Pharmazeutische Chemie, Johann-Wolfgang Goethe Universität Frankfurt, Biozentrum, Marie-Curie Strasse 9-11, D-60439 Frankfurt am Main, Germany

Abstract

The present paper reports detailed studies on the internal energy of matrix-assisted laser desorbed ions using delayed extraction MALDI-TOF and atmospheric-pressure MALDI. We used benzylpyridinium cations as internal energy probes. Our study reveals three distinct contributions to internal energy build-up in vacuum-MALDI (classical MALDI-TOF), each one having different effects on ion fragmentation. Some fragments are formed before ion extraction (i.e. maximum 100 ns after the laser impact), and are therefore well resolved and sharp in the MALDI-TOF MS scan. This prompt fragmentation can have two origins: (i) in-plume thermal activation, presumably always present, and (ii) in-plume chemical reactions with hydrogen radicals. In addition to these promptly formed fragments, a broad peak slightly offset to higher masses could be detected, corresponding to fragments formed after the extraction has started. A third source of internal energy for MALDI ions is therefore (iii) the extraction-induced collisional activation of the ions with the neutral components of the plume. These three contributions are difficult to quantify in vacuum-MALDI, because of the combined influence of several parameters (nature of the matrix, spot-to-spot variability, total laser exposure, delay time, acceleration voltage) on extraction-induced fragmentation. Atmospheric pressure MALDI has two advantages for comparative studies of analyte fragmentation. First, extraction-induced fragmentation is absent, and only the contribution of early plume activation remains. Second, the reproducibility is far better than in vacuum-MALDI. AP-MALDI is therefore expected to shed a new light on the early steps of the MALDI process.

[†] Present address : Mass Spectrometry Laboratory, Chemistry Department, University of Liège, Institut de Chimie, Bat. B6c, B-4000 Liège, Belgium.

Abbreviations

Matrices:

ATT: 6-azathiothymine

CHCA: α-cyano-4-hydroxycinnamic acid

DHB: 2,5-dihydroxybenzoic acid

DHBs: 90% 2,5-dihydroxybenzoic acid/10% 2-hydroxy-5-methoxybenzoic acid

HPA: 3-hydroxypicolinic acid (3-hydroxypyridine-2-carboxylic acid)

p-NA: para-nitroaniline

SA: sinapinic acid (3,5-dimethoxy-4-hydroxycinnamic acid)

Others:

BzPy: benzylpyridinium

CE: continuous extraction

DE: delayed extraction

ISD: in-source decay

PSD: post-source decay

Introduction

A better understanding of the matrix influence on ion fragmentation could lead to more "tailor-made" sample preparations, depending on the application. While softness is required for molecular mass determination, extensive fragmentation is advantageous for structural studies, and particularly for peptide sequencing. Moreover, the investigation of the different contributions to analyte excitation and fragmentation would be a privileged way to get some insight into the mechanisms of MALDI, and in particular into what has made the method so popular: its softness. Our goal here is not to make a review of the different models proposed for the MALDI mechanism, and the reader is encouraged to refer to recent reviews for these subjects[1-4]. Rather, we will focus on the internal energy aspects of MALDI.

In the early days[5-8], it was generally believed that MALDI was a very soft ionization method capable of transferring intact molecular ions into the gas phase without fragmentation. The advent of reflector-type analyzers allowed to emphasize that metastable decay did actually occur in MALDI (fragmentation during the ion flight in the mass analyzer). When the mass of the fragment is 85 to 90% of the parent ion mass, the fragments can be resolved directly in normal reflector mode MALDI. Such fragmentations are quite prominent in oligodeoxynucleotides (neutral base loss)[9-12], acetylated peptides (CH_2O loss)[13], phosphopeptides/proteins (H_3PO_4 and HPO_3 losses)[13,14], and glycopeptides/proteins (carbohydrate loss)[15,16]. In the case of large proteins, these multiple neutral losses (and probably also water and ammonia losses) are responsible for a low-mass tail which is detrimental to the mass resolution. Smaller fragments however need adjusting the voltages of the ion mirror in order to be focused on the detector[17,18]. This operation mode is often referred to as "post-source decay" (PSD)[18,19]. In the following, "metastable decay" encompasses both PSD and neutral losses. Metastable decay characteristics are reviewed in ref.[19]. Briefly, fragmentation efficiency is enhanced when (1) the laser power is increased[20], (2) the acceleration field strength is increased, (3) the residual gas pressure is increased[18], and (4) continuous rather than delayed extraction is used. It was therefore concluded that metastable decay resulted from collisional activation of the analyte with the matrix plume upon acceleration in the source[19,21]. The choice of the matrix

also plays an important role in the fragmentation and the propensity to cause fragmentation, both in PSD and in metastable neutral loss, is consistently found to rank in the following way: CHCA > SA > DHB > DHBs ≈ ATT > salicylic acid ≈ HPA[9,13,15,16,18]. The former matrices are therefore called "hot" and the latter "cold".

In-source decay (ISD)[22-30] shows drastically different characteristics than PSD. The fragments are observed in both linear or reflector mass spectra, and can be observed with delayed extraction with delay time as short as 38 ns[31], and even in continuous extraction[25,31]. The fragments are therefore formed in the source, a few tens of nanoseconds after the laser irradiation. In the case of peptides and proteins, ISD is characterized by the presence of *c* (and occasionally *z*) ions, in addition to some *a*, *b* and *y* ions which are commonly observed in PSD. It is generally believed that ISD ions form due to hydrogen radical transfer from the matrix to the analyte in the dense plume[30,32], a process which has some analogies with electron capture dissociation (ECD)[33]. The same fragment ion spectrum is observed both in the positive and the negative ion mode, indicating that ISD is independent of ionization, and hence on proton transfer[25]. The matrix which is the most prone both to hydrogen radical transfer and to ISD is DHB[25,30-32,34]. ISD fragmentation is dramatically reduced in DHBs[25]. Ferulic and sinapinic acid were found to produce satisfactory ISD signal by some authors[23-25], but not by others[31]. In strong contrast with PSD, the CHCA matrix is found to be inefficient in producing ISD fragments[25].

Only a few experimental determinations of ion internal energies in MALDI have been reported to date. Photoionization studies of matrix-assisted laser-desorbed *neutrals* have been performed, allowing the internal energy to be quantified from the degree of metastable decay in the photoionization spectra[35,36]. Neutrals' temperature was found in the range 400-500 K[36], which has long been interpreted as a proof that ion internal energies are determined by the matrix sublimation temperature. The temperature increases with the laser irradiance, but is independent on the probe temperature. Moreover, the neutrals at the front of the plume are hotter than those lagging behind. Stevenson et al.[37] used the fragmentation of the dinucleotide anion AG as a probe of the internal energy, but no quantification could be made. They found that the matrix dependence of ion internal energies (p-NA > SA > DHB ≈ THAP > CHCA) is consistent with the exothermicity of the proton exchange reaction between the analyte and the matrix, and inconsistent with the sublimation

temperatures. Other authors also suggested that the chemical reactivity of the matrix, and in particular its gas-phase basicity or proton affinity, could also dramatically influence the analyte fragmentation[3,10,15,16,21,37]. It is remarkable that the order of fragmentation observed by Stevenson et al.[37] is not the same as observed for peptides and proteins in metastable decay (CHCA > SA > DHB). It must be pointed out that the ions are produced in the internal source of an FTICR mass spectrometer, and the ions are allowed to drift for 2-500 µs before any trapping voltage is applied, so the experimental conditions are therefore significantly different from typical metastable decay conditions. Luo et al.[38] recently reported the first quantification of *ion* internal energies produced by MALDI from the fragmentation yields of benzylpyridinium ions. These ions were used previously by De Pauw et al. for the quantification of internal energy input in electrospray ionization[39-41]. The experiments were performed in continuous extraction linear mode, and consequently the detected fragments are formed very shortly after laser excitation. Assuming a fragmentation time of 100 ns, the authors found mean ion internal energies of 3.7 eV for CHCA, 4.0 eV for SA, and 4.3 eV for DHB. To make comparisons easier, this corresponds to internal temperatures of 1180 K, 1235 K, and 1295 K respectively. The ion internal energy was found to increase with the laser fluence, so the relative ordering of the matrices in terms of hardness/softness depends on the fluence. Again, the fragmentation conditions are very different from metastable decay experiments (prompt fragmentation in continuous extraction linear TOF experiments vs. fragmentation in the flight tube in reflector mode or PSD experiments). The benzylpyridinium thermometer ions were also used by Greisch et al.[42], who characterized the ion internal energy by an effective temperature instead of an effective energy, but the matrices used are not typical of MALDI conditions. The effective temperatures were around 1360 K and 1490 K for $NaNO_3$ and NH_4CO_3, respectively.

The models accounting for the internal energy of MALDI ions also evolved with time. In the early days, an energy bottleneck model[43,44] was proposed to account for the supposed absence of analyte fragmentation. According to this model, a frequency mismatch between the lattice vibrations and the analyte vibrations slows down the lattice-to-analyte energy transfer, and the lower the sublimation temperature of the matrix, the faster the desorption. The analyte temperature is therefore lower than the matrix temperature at the time of desorption. However, now it is generally admitted that substantial overheating of the matrix above its sublimation temperature is

achieved, leading to coherent desorption of the matrix and the analyte[1]. The interesting aspect of the model is that the analyte internal temperature should be correlated to the matrix sublimation temperature. Later, a hydrodynamic model of the plume expansion was proposed[45], according to which the analyte internal energy cools down due to the adiabatic expansion of the dense plume in vacuum. The authors predicted a cooling of the analyte temperature even below room temperature. If this model were valid, then the analyte internal temperature should be correlated to the mean ion velocities[46]. In 1995, Dreisewerd at al.[47] found that the ion signal dependence on the laser fluence could be fitted by a quasi-thermal sublimation/desorption model, where the system temperature is given by

$$T = T_0 + \eta H \quad (1)$$

where T_0 is the initial temperature, H is the laser fluence, and η is the conversion efficiency of laser energy into a temperature increase. The lowest system temperature T is found at threshold and for large spot sizes. For the photoionized matrix neutrals, T_{min} is 464 K, while for the laser-desorbed matrix ions, T_{min} is around 900 K. More recently, the internal temperature has been addressed by computer simulation. Knochenmuss proposed a quantitative model of MALDI[48], considering the MALDI sample as a continuous medium for which a temperature can be defined. The model accounts for the conversion of electronic energy to heat, and supposes that desorption starts once the temperature becomes superior to the matrix sublimation temperature (450 K for DHB). DHB plume peak temperatures were found around 525-550 K. Molecular dynamics simulations allow to take non-equilibrium effects into account[49-51]. Benscura et al.[49] predict internal temperatures higher than room temperature (350 to 800 K), but always lower than the temperature jump in the lattice. Zhigilei et al.[4,50,51], who combined MD simulations at short time scales with direct simulation Monte Carlo at long time scales, investigated the internal temperatures of ejected clusters. Large clusters remain hotter than small ones. For thermal confinement conditions (laser pulses longer than 50 ps), the cluster temperatures were between 400 and 900 K.

The understanding of the MALDI process and the refinement of existing models would greatly benefit from additional experimental results on MALDI ion temperatures for different types of analytes. In the present paper, we report an experimental study of the fragmentation of benzylpyridinium ions as thermometer

molecules in delayed extraction vacuum-MALDI. We used continuous and delayed extraction with different delay times, and could distinguish the contributions of prompt fragmentation occurring shortly after irradiation from the processes induced by collisions induced by extraction from the source. We also performed a comparative study between vacuum-MALDI and atmospheric-pressure MALDI (AP-MALDI).

Experimental section

Materials

The benzylpyridinium compounds were synthesized by reflux of the corresponding benzylchlorides in pyridine (all from Aldrich), and purified by re-crystallization. The samples were diluted to 10^{-4} M in H_2O/CH_3CN 50/50. The dipeptide Val-Pro and the deoxynucleotides were obtained from Sigma. α-cyano-4-hydroxycinnamic acid (CHCA) was obtained from Fluka, 2,5-dihydroxybenzoic acid (DHB) from Acros and sinapinic acid (SA) from Aldrich (98%) and Applied Biosystems ("ultra pure" – Lot 0205007). DHB was dissolved at 20 mg/ml in H_2O/CH_3CN 50/50. The matrix solutions of CHCA and SA were saturated solutions in H_2O/CH_3CN 50/50. The MALDI spots were prepared according to the dried-droplet method (1 μL + 1 μL). The droplets are allowed to dry under a gentle stream of cold air. In the case of DHB, the large crystals on the rim of the spot were used for the experiments, in order to use similar conditions as those typically used for peptide/protein analysis. For one series of AP-MALDI experiments, DHB spots were prepared by vacuum drying to produce a homogeneous layer of small crystals.

Instrumentation

MALDI-TOF experiments were performed on a Voyager DE-PRO (Applied Biosystems, Framingham, MA). The voltage on the second grid is equal to 0. Before extraction, the voltage on the target plate and on the first grid are both equal to GU (G is a constant between 0 and 1). When extraction starts, the voltage on the plate is set to U, so that the voltage difference between the plate and grid 1 is equal to $(1-G)U$. Unless otherwise mentioned, the parameters used were U = 20 kV, G = 0.96. The minimum extraction delay time on the instrument is 200 ns. The laser is a N_2 laser with wavelength 337 nm and a pulse width of ≈ 3 ns.

AP-MALDI experiments were performed on an Agilent 1100 series LC/MSD trap SL. The nitrogen laser (337 nm) produces a 10 Hz pulsed beam, with a pulse width of ≈ 3 ns. The laser energy has been measured with a NOVA Laser Power/Energy Monitor (Ophir Optronics Ltd, Jerusalem, Israel). The area of the

irradiated surface is $(2.59 \pm 0.08) \times 10^{-3}$ cm². The analytes formed during the MALDI event are dragged through the capillary extension toward the glass capillary. A stream of nitrogen gas flowing at 5 l/min. was heated to 150 °C. High voltage (4.0 kV) was applied to the capillary extension. The capillary exit voltage was set to 50 V, the skimmer to 15 V, the octapoles 1 and 2 DC voltages to 8.0 and 2.5 V, respectively. The maximum accumulation time during which ions were gated into the trap was set to 600 ms. Actual accumulation time was determined by the ion charge control (ICC), which was set to limit the abundance to 30000 counts. The trap scanned from 50 to 500 Th. Spectra were acquired for 2 min and averaged. The trap drive was set to 25 to avoid mass-dependent discrimination. All instrumental parameters were tuned with the benzylpyridinium ions in electrospray, to ensure that minimum fragmentation occurs due to collisional activation in the source or upon trapping.

Determination of the effective temperatures

The effective temperatures were determined as described previously[41,42]. The dissociation rate constants $k(E)$ were calculated with the RRKM equation (Eq. 1).

$$k(E) = \frac{G^{\ddagger}(E - E_0)}{hN(E)} = \frac{\int_0^{E-E_0} N^{\ddagger}(E_u)dE_u}{hN(E)} \qquad (1)$$

where E_0 is the difference between the zero point energy of the transition state and the zero point energy of the reactant, $G^{\ddagger}(E - E_0)$ is the number of states of the transition state whose energy lies in the range $[0, E - E_0]$, h is the Planck constant, and $N(E)$ is the density of states of the reactant at energy E. The benzylpyridinium ions fragment according to Scheme 1[39-41,52,53]. All energy and vibrational frequency calculations were performed with Gamess US at the *ab initio* HF/6-31G* level. Vibrational frequencies computed by ab initio Hartree-Fock methods are usually overestimated compared to the experimental values[54]. For the method used here, a scaling factor of 0.89 was used. The vibrational frequencies of the transition state were calculated from those of the reactant by eliminating the frequency corresponding the most closely to the N^+—CH_2 bond vibration, and by scaling five other frequencies

(two at ≈ 800 cm^{-1}, two at ≈ 600 cm^{-1}, and one at ≈ 100 cm^{-1}) by a factor of 0.75. This scaling is a convenient way of simulating a loose transition state[55]. The threshold energies E_0 for fragmentation were calculated as the energy difference between the zero-point energy of the fragments (pyridine + benzyl) and the zero-point energy of the benzylpyridinium ion. The density of states $N(E)$ were computed by direct state count. The relationship between the survival yield and the effective temperature is calculated by Equation (2)[41], where $P(E;T)$ is the Boltzmann distribution at the temperature T (Equation 3), and the dissociation time τ was assumed to be 100 ns (see discussion in the text).

$$SY(T) = \frac{I(M^+)}{I(M^+)+I(F^+)} = \int_0^\infty P(E;T)e^{-k(E).\tau}dE \qquad (2)$$

$$P(E;T)=\frac{N(E)e^{-E/kT}}{\int_0^\infty N(E)e^{-E/kT}dE} \qquad (3)$$

Results

MALDI-TOF MS (vacuum-MALDI)

Dissociation of the benzylpyridinium ions

Initially, our goal was to measure the survival yields of the benzylpyridinium (BzPy) ions in different matrices, and to calculate the ion effective temperatures. However, we noticed that, in the delayed extraction mass spectra, the fragment ion peak shape was quite unusual. Typical spectra obtained for p-OCH_3 BzPy with DHB in continuous extraction linear mode and delayed extraction linear and reflector modes are shown in Figure 1. In the delayed extraction linear mode (Fig. 1b), the benzyl fragment shows a sharp peak at the correct mass (and therefore at the correct arrival time, the calibration being done on matrix peaks), but also a broad peak offset by ~ 1 Da toward higher masses. In the delayed extraction reflector mode, this broad peak is still visible, but now shifted by only ~ 0.6 Da. This excludes the assignment of this peak to $FH^{\bullet+}$. Measuring the time shift instead of the mass shift between the sharp and the broad component of the fragment peak gives a flight time shift of ~ 30 ns (maximum to maximum) in both the linear and the reflector mode. This suggests that the broad component is due to fragments F^+ arriving ~ 30 ns later than the regular fragments at the detector. We will call this peak the "delayed peak". We checked that this was not simply an instrumental artifact by performing the same experiments with a Voyager DE-STR (Applied Biosystems, Framingham, MA) and a UltraFlex TOF-TOF MALDI mass spectrometer (Bruker, Bremen, Germany). The same peak shape was observed (data not shown). We investigated in more detail the influence of several parameters on the fragment ion peak shape, namely the influence of the matrix, the laser fluence, the total laser exposure, the time delay between laser impact and extraction, and the extraction voltage. Because of the limited dynamic range of the instrument, we focused on the ratio between the sharp and delayed peak, and not on their relative intensities compared to the parent ion.

The influence of the laser exposure on the fragment ion peak shape is shown in Figure 2 for sinapinic acid (SA) and α-cyano-4-hydroxycinnamic acid (CHCA). For these two matrices, the crystallization is quite homogeneous, and the spectra have been acquired by scanning the same area of the spot for each value of the laser

intensity. The laser intensity was first increased, then decreased. Increase of the laser power always results in an increase of the relative intensity of the delayed peak. For SA (Fig. 2a), the subsequent decrease of the laser power gives a reversible decrease of the proportion of "delayed" fragments, while for CHCA (Fig. 2b), there is a remarkable hysteresis effect. The cumulated laser exposure has therefore an influence on ion fragmentation. The case of DHB is more difficult to investigate in a reproducible manner, due to the high crystal-dependence of the ion signal. We wanted to concentrate our attention to the outer rim big crystals of the dried droplet preparation because these are the typical conditions used for peptide and protein analytes. We also noticed that the sharp/delayed peak ratio highly depends on the choice of the crystal. Unfortunately, the ion signal on a single crystal was not persistent enough to perform a reproducible laser exposure study such as in Figure 2, but the general trend is shown in Figure 3. Figure 3a shows the first spectrum acquired on a fresh DHB spot, close to threshold. We then performed several measurements on this spot, at the same and at higher laser power. We then set the laser intensity to its initial value and tried to find a spot giving the same spectrum as in Figure 3a. This was found impossible. A typical spectrum obtained at threshold, but after extensive laser irradiation is shown in Figure 3b: the proportion of delayed fragments is higher after laser exposure.

The influence of the delay time at a given laser fluence is shown in Figure 4 for SA (Fig. 4a) and CHCA (Fig. 4b). The laser intensity was chosen high enough to have a detectable signal at long delay time, and to favor the formation of delayed fragments. In the case of sinapinic acid, the results were not quantitatively reproducible, due to the low ion signal at long delay times, but in all cases, significant contribution of the delayed fragment can still be seen at a delay time of 1000 ns. The same kind of result is obtained for DHB, but again the spot-to-spot variations are large. In contrast, for CHCA (Fig. 4b), the fraction of "delayed" fragments markedly diminishes when the extraction delay time is increased. At 1400 ns, only the sharp fragment peak remains.

The influence of the extraction voltage can be studied by varying the value of G, as the voltage between the plate and the first grid is equal to $(1\text{-}G)U$. Lowering G therefore increases the extraction voltage. The influence of G on the fragment ion peak shape, both in linear and reflector mode, is shown in Figure 5 for p-CH_3 BzPy in CHCA (delay 200 ns). The sharp and the broad component of the peak become closer

as *G* increases. In the linear mode, the two peaks can even not be differentiated when $G \leq 0.92$ The difference in flight times between the maxima is similar in the linear and the reflector mode, although it can be determined more precisely in the reflector mode.

Another detail that was already mentioned, but not discussed, in a previous study of Vertes et al. is the presence of a fragment at 80 Da (Figures 1 and 3), corresponding to protonated pyridine. This fragment can not be observed in ESI, nor in low-energy CID of benzylpyridinium ions. PyH^+ can not be observed in LDI (without matrix) or in matrix-enhanced LDI (ammonium hydrogenocarbonate or sodium nitrate as matrices). The matrix propensity to form such fragment is in the order: DHB >> SA > CHCA. In DE-MALDI-TOF, the peak shape reveals only a sharp component in all instrumental conditions. For DHB, the laser exposure also has an influence on the relative proportions of PyH^+ and F^+ fragments: after some laser exposure (Fig. 3b), the PyH^+ ion becomes more abundant.

Dissociation of the peptide Val-Pro

We also tested some other small fragile molecules to check that the peak shape observed for the benzylpyridinium ions is not an isolated case. We made some tests with deoxynucleosides, but we could not detect a broad component of the fragment peak. However, the fragmentation of the small peptide Val-Pro[56] reveals the same effect on its two fragments a_1 and $y"_1$ (Figure 6). The effect of *G* is similar as for the benzylpyridinium, and the relative proportion of sharp and delayed fragments is different for the two fragments.

Atmospheric pressure MALDI

In atmospheric pressure MALDI coupled to a quadrupole ion trap, signal saturation is avoided by controlling the number of ions allowed inside the trap. Each parent or fragment ion has the same peak shape, as there is no memory of the time of flight of the ions from the source to the analyzer. We could measure the survival yields (fraction of intact molecular ion, see Eq. 2) of the three benzylpyridinium ions p-CH_3, p-OCH_3 and p-tBu at the same time, as the parent and fragment ions all have different masses. In AP-MALDI, the amount of fragments was sometimes very low (high survival yields). Figure 7 shows such an example. The fragment ion of p-CH_3

has a very low intensity. For each spectrum we carefully checked that there was no interference with matrix peaks. Fortunately, no one of the major matrix peaks had the same mass as the different M^+ and F^+. When a minor interference was found, the relative intensity of the interfering peak was measured as compare to a major matrix peak in a spectrum of the neat matrix, and this ratio was used to substract the intensity of the interfering matrix peak from the intensity of the ion of interest.

Figure 8 shows the survival yields measured for the three probe ions with the different matrices as a function of the laser fluence. The error bars represent the standard deviations of at least 3 replicate experiments. The same survival yields are found when different modes of preparation are compared for a given matrix. For CHCA, there is no influence of the nature of the metal target on the survival yield. For DHB, the survival yields are obtained for large crystals in dried droplet preparation as for small crystals obtained by vacuum drying. For SA, the same results are obtained for the ultrapure matrix (white powder) as for the 98%-quality matrix (pale brown powder).

Discussion

Vacuum-MALDI-TOF: fragment ion peak shape

In order to determine the origin of the delayed fragment peak, let us first examine the different regions of the mass spectrometer where fragmentation can occur, and the corresponding time scales. Figure 9 shows a scheme of the Voyager DE-PRO instrument. First, fragments can form during the delay time between the laser shot and the onset of the extraction voltage. This is also the time window where matrix and analyte ionization occurs. In the case of the benzylpyridinium cations, we suppose that the cations are already present in the matrix crystals. The spectra are calibrated with the matrix peaks, which are sharp. Therefore the sharp fragment peak (at the right *m*/*z* value) is due to fragments formed before extraction. We will call them the "prompt" fragments. Second, once the extraction starts, the parent ions that survived are accelerated between the plate and grid 1 at a relatively low potential difference (for U = 20 kV and G = 0.96, the potential difference is $(1\text{-}G)U$ = 800 V). Third, the parent ions that fragment between grids 1 and 2 (for U = 20 kV and G = 0.96, the potential difference is GU = 19.2 kV) can not be detected. In the mass spectrum, they contribute to the noise between the fragment and the parent ion peaks. In order to be detected intact, the parent ions must have survived up to the field free region (FFR) of the mass spectrometer (in the linear mode).

To correlate the place and time of fragmentation to the fragment arrival time, we used a simple kinematics model, based on the voltages and distances given in Figure 9. After the laser pulse, the ions are allowed to move freely with an initial velocity v_0, during the extraction delay time, and cover a distance x_d. The initial velocity was assumed to be equal to 400 m/s (modeling shows that this value does not have a significant influence on the difference in flight times). When extraction starts, the parent ions undergo an acceleration a_A (Equation 4), where q is the ion charge in Coulomb ($q = z \times e$), G, U and d_1 are defined above (see Figure 9), and m_M is the mass of the parent ion.

$$a_A = \frac{q(1-G)U}{d_1 m_M} \qquad (4)$$

If fragmentation occurs before passing grid 1, i.e. at a distance $x_f < d_1\text{-}x_d$ from the ion position where extraction started, the potential difference remains unchanged, but the magnitude of the acceleration of the resulting fragment is different due to the lower mass of the fragment ($m_F < m_M$). In region B, the acceleration is given by:

$$a_B = \frac{q(1-G)U}{d_1 m_F} \quad (5)$$

In region C (between grid 1 and grid 2), the acceleration is given by:

$$a_C = \frac{qGU}{d_2 m_F} \quad (6)$$

Finally, in the field free region, ions simply continue to travel at the velocity they reached at grid 2. These simple kinematics considerations allow to calculate the theoretical total flight times of the fragment ion as a function of the distance x_f at which it forms. The model does not include any recoil upon collision. The results of this modeling are shown in Figure 10 for p-OCH_3 BzPy in DHB. The theoretical flight time of the prompt fragment is calculated to be 7475 ns, in good agreement with the experimental value (7349 ns), given the simplicity of the kinematics model. The mass spectrum (Fig. 10a) can be converted back to a time spectrum, knowing the instrument calibration. The difference in flight time as compared to the prompt fragments is shown in Figure 10b. Then, the kinematics model is used to correlate the difference in flight times to the time t_A after extraction at which the fragment is formed (Fig. 10c), or alternatively to the distance x_f the parent ion M^+ covered before fragmenting (Fig. 10d). This shows that the delayed fragment peak could correspond to fragments formed during the first extraction stage (between the plate and grid 1).

The observation of a sharp and a broad component in the ion peak shape may recall the observations of Kinsel at al.[57], who interpreted their results by invoking two components in ion *formation* (prompt ionization and delayed gas-phase ionization by reactions with the plume). However the situation is completely different here, as the two-component peak shape is observed only for the fragment, in delayed extraction, while the study of Kinsel et al. was performed in continuous extraction, and concerned the molecular ions. We used quaternary ammonium ions especially to avoid any speculative considerations on analyte ionization. Here we therefore interpret our results by invoking two components in the ion *fragmentation*. Figure 9 shows that the fragment peak shape can be explained by (i) one fraction fragmenting

before extraction and (ii) one fraction fragmenting after extraction has started. The most plausible explanation is that, when extraction starts, ions are dragged through neutral components of the plume, and that the collisions between the analyte and the plume are at the origin of the fragmentation.

Vacuum-MALDI-TOF: fragmentation kinetics

It is quite common to observe fragment ion peak shapes showing a high-mass tail, indicating that fragmentation which started during the extraction delay continues during extraction. What is surprising in the peak shape observed here is that the sharp and the broad component are clearly decoupled, even at the minimum delay time of 200 ns. The decoupling indicates that the prompt fragmentation is already finished when extraction starts. The fragments contributing to the sharp peak must have been formed in a shorter time scale than 200 ns. We will assume that the fragmentation time scale is < 100 ns. In terms of internal energy distribution, this means either that the ions cool down (the P(E) changes) in a time scale shorter than 100 ns, or that the internal energy distribution acquired just after laser impact is bimodal (a high energy and a low energy component). Once the surviving parent ions are extracted, they receive again a considerable amount of internal energy, causing fragmentation in the 10-100 ns time scale.

The position of the delayed peak is not changing when changing the matrix, the extraction delay time, or the laser intensity (see Figures 2-4), so the time elapsed between ion extraction and fragmentation is not changing, but the relative proportions of prompt-to-delayed fragments are changing. We suggest that the proportion of delayed fragments depends on the collision probability during extraction, and therefore on the density of the plume when extraction takes place. The ion mean free path λ can be related to the pressure *p* with Equation (7), considering that the ion and the matrix molecules in the plume have roughly the same size (parameter σ).

$$\lambda = \frac{RT}{\pi\sqrt{2} \cdot p \cdot N_A \cdot \sigma^2} \qquad (7)$$

In order to have a mean free path of 0.2 mm (an average of one collision between the plate and grid 1), the pressure of the matrix plume should be 2×10^{-3} mbar (considering σ = 10 Å, and T = 300 K). The pressure inside the mass spectrometer is

10^{-6} mbar. An average of less than one collision with the plume between extraction and grid 1 will be assumed in the following discussion.

The position of the delayed fragment peak is changing with the ion extraction voltage, determined by the value of *G*. The formation time t_A and formation place x_f extracted from the spectra of Figure 5 are summarized in Table 1. The proportion of delayed fragments seems to increase when *G* decreases. The calculation of the time elapsed between extraction and fragmentation gives information on the kinetics of this extraction-induced fragmentation. It must be emphasized that the observed distribution of fragment intensity as a function of fragmentation time t_A is a convolution of different distributions:

(1) the place where the collision(s) occur(s),

(2) the amount of kinetic energy transferred into internal energy in each collision,

(3) the energy-dependent dissociation rate constant, which can be calculated using the RRKM equation (Eq. 1).

Consequently, a detailed modeling of the ion activation and dissociation is not feasible just from the information contained in the mass spectra, and we therefore use the simplified view of a single collision. We tested whether the observed dissociation kinetics could be compatible with a single collision giving rise to an ergodic dissociation (re-distribution of the internal energy on all the degrees of freedom before fragmentation) for which the rate constant is given by the RRKM equation (1).

First, the high collision energies encountered in MALDI-TOF are compatible with the fast dissociation observed. The relative kinetic energy of the collision in the center-of-mass frame of reference can be calculated with Equation (8),

$$KE_{rel} = \frac{m_M m_{matrix}}{m_M + m_{matrix}} \cdot \frac{(v_{lab} - v_0)^2}{2} \qquad (8)$$

where m_M and m_{matrix} are the masses of the analyte and of the matrix respectively, v_{lab} is the ion velocity in the laboratory frame of reference (calculated with the kinematic model described above) and v_0 is the initial velocity, assumed to be the velocity of the neutrals. The relative velocity of the collision is equal to $(v_{lab} - v_0)$ because both the ions and the matrix travel in the same direction. If the mass of the neutral target is larger (a matrix cluster for example), the relative collision energy will be even higher. Figure 11 shows the relative collision energy as a function of the distance x_f covered by the parent ion. It is clear that the influence of G on the relative collision energy

(Fig. 11) correlates well with the observed coalescence of the broad and the sharp peak observed experimentally (Figure 5 and Table 1). Fragmentation occurs when the relative collision energy reaches ca. 30 eV. So, even if the conversion of relative kinetic energy into internal energy has not 100% efficiency, the fast fragmentation kinetics observed ($\approx 10^7$ s^{-1}) is theoretically possible.

However, the difference in flight times, and hence the formation time t_A, does not change significantly with the nature of the substituent at a given G value, even thought the fragmentation thresholds energies are quite different. This observation is in contradiction with the RRKM rate constants (Figure 12), according to which the internal energies (and therefore the collision energies) at which the fragment appears whould vary from molecule to molecule. For example, in order to have a dissociation rate of 10^7 s^{-1} (half life of ≈ 60 ns), an the parent ion internal energy should be 3.8 eV for p-OCH_3, 5.3 eV for p-CH_3, and 6.5 eV for p-tBu. This observation can be rationalized if it is assumed that, at a critical relative collision energy (30-35 eV), the collision between the analyte and the matrix causes a fast energy transfer directly in the reaction coordinate, resulting in an apparently immediate fragmentation. Such non-ergodic dissociation is not so unrealistic in the case considered here, where the collision partner (a matrix molecule) is of similar size as the analyte ion. Let us imagine the dynamics of such a collision: if the matrix molecule hits one of the two aromatic cycles of the benzylpyridinium, there will be a huge recoil of one aromatic cycle relative to the other, and thereby an elongation of the N^+—CH_2 bond, which is precisely the reaction coordinate. This kind of fast, non-ergodic dissociation upon collision-induced dissociation is quite uncommon in mass spectrometry, where the target is usually a mono- or diatomic gas (He, Ar, N_2,…), but has already been observed when the target has a high mass, like in the surface-induced dissociation (SID) of peptides. This non-ergodic dissociation has been called “shattering”[58,59].

Last but not least, it must be noted that, while the collision-induced fragmentation in the plume is a fast process, the parent ion M^+ is still detected with a large relative intensity, both in the linear and the reflector mode, meaning that only a fraction of the parent ions did actually undergo this kind of collisions, and this is also an indication that the parent ions undergo less than one collision on average. This fraction will depend on the plume density, and therefore on the choice of the matrix,

and on the delay time. It is hoped that further work on fragment ion peak shape analysis could be used to probe the plume dynamics.

Vacuum-MALDI-TOF: the different contributions to internal energy build-up

Table 2 summarizes the different contributions to internal energy build-up, and their respective consequences in terms of fragmentation in the case of the benzylpyridinium ions. The sharp fragment peaks correspond to fragments formed shortly (≤ 100 ns) after laser impact. The molecular ions receive this internal energy either directly from the laser, or by the intermediate of the matrix. This is the process of interest to obtain useful information on the MALDI mechanism. In all previous low-energy dissociation studies performed on benzylpyridinium cations (electrospray source-CID, Q-TOF or ion trap MS/MS), the only fragment observed has always been the benzyl cation F^+. However, in MALDI, the observation of PyH^+ is an indication of the presence of an additional process. This fragment is attributed to hydrogen radical chemistry in the plume. The reaction is shown in Scheme 2. The hydrogen radical attacks the positively charged center of the pyridinium ion, causing a homolytic cleavage of the N^+—CH_2 bond. The radical fragment is stabilized by the aromatic ring. The presence of hydrogen radicals in the MALDI plume has been reported in several cases[30,32,34] (mostly with DHB), and is thought to be at the origin of the in-source decay (ISD) of peptides. For peptides, the matrix relative propensity to form the characteristic ISD "c" and "z" fragments is DHB > SA >> CHCA[23-25,31], as we observed for the BzPy ions. Furthermore, ISD is a fast process[25,31] (time scale < 40 ns), which is in agreement with the observed sharp peak observed for PyH^+.

The delayed fragment peak corresponds to fragments formed 10 to 100 ns after the onset of the extraction field. This fragmentation channel is favored (1) when the laser power is increased, (2) when the extraction field strength is increased, (3) when the extraction delay time is shortened. These three characteristics are similar to the characteristics of metastable decay of peptides, proteins and oligonucleotides. Indeed, metastable decay is supposed to result from collisional activation of the analyte with the matrix plume upon acceleration in the source[19,21]. With the small molecules we investigated, we found a very fast fragmentation, which may even be non-ergodic,

due to the comparable size of the analyte and of the neutral collider, the matrix. However, as the size of the analyte increases, it is likely that the non-ergodic character will disappear, and that the fragmentation will proceed on a longer time scale. So, it is plausible that the delayed fragments observed here, and the metastable fragmentation commonly observed for peptides, proteins, and oligonucleotides, both result from the same process.

In the paper of Luo et al.[38], the experiments on the benzylpyridinium ions were performed in continuous extraction mode. The mean internal energy was calculated using the relative intensities of M^+ and F^+, RRKM unimolecular rate constants, and assuming a reaction time of 100 ns. The results are therefore representative of the sum of the contributions of the prompt laser-induced fragmentation and of the extraction-induced fragmentation. We show here that, for a given extraction delay and extraction field, the relative contribution of these two processes greatly depends not only on the matrix and on the laser fluence, but also on the total laser exposure. The resulting crystal-to-crystal variability explains that large error bars are obtained when measuring the benzylpyridinium ions' survival yield and internal energy. Furthermore, the extraction-induced fragmentation may not be well described by the RRKM dissociation rate constants, as discussed above.

Atmospheric pressure MALDI

From all the considerations described above, it is clear that the characterization of the relative matrix hardness/softness using benzylpyridinium ions as thermometer ions is extremely complicated in vacuum MALDI-TOF because different processes contribute to the final mass spectrum. We believe that the contribution of the prompt fragmentation processes could eventually give the most insight into the heart of the MALDI process: how the laser energy is transferred into analyte kinetic energy (essential for efficient ion desorption) and internal energy (a side effect to be avoided in some cases, or to promote in others). All collision-induced processes and metastable dissociation occurring upon extraction in TOF instruments are shielding this process. We therefore investigated the case of AP-MALDI. In this case, the numerous collisions with nitrogen at atmospheric pressure slow down the ions, preventing any high-energy extraction-induced fragmentation like in vacuum-

MALDI. This is the first advantage of AP-MALDI. The better reproducibility of AP-MALDI (smaller standard deviations on the survival yields measured in AP-MALDI, compared to vacuum-MALDI[38]) is a second advantage when making comparisons, for example between matrices.

Using RRKM calculations, the survival yield can be correlated to the ion effective internal energy (the internal energy of an ion that would fragment with the same rate as the ion population under investigation), or to the ion effective temperature (the temperature of the Boltzmann energy distribution of an ion population that would fragment with the same rate as the ion population under investigation). At this stage, this definition does not give a physical meaning to the ion effective temperature[60,61]. If all three benzylpyridinium ions would have the same effective internal energy and if their fragmentation was ergodic (the non-ergodic behavior concerns *a priori* only the extraction-induced fragmentation, which is not the case here), their survival yields would be determined by the RRKM dissociation rate constants (Figure 11). The survival yields would rank, from highest to lowest: p-tBu > p-CH_3 > p-OCH_3. However, we observe that the survival yields (Figure 8) rather rank according to the threshold energies E_0: p-CH_3 > p-tBu > p-OCH_3. This suggested that, rather than having the same total internal energy, the ions have a similar amount of internal energy per degree of freedom, which means a similar temperature. For each ion, the effective temperature is calculated assuming a reaction time of 100 ns. This time scale has been chosen quite arbitrarily, as the time required before cooling by collisions at atmospheric pressure is not known. We used the same time scale as for the vacuum-MALDI study of Luo et al.[38], for a purpose of comparison. The results are presented in Figure 13.

Figure 13A shows that the p-CH_3 and p-tBu benzylpyridiniums have the same effective temperature within experimental error, although these molecules have different numbers of degrees of freedom, different RRKM rate constants (Fig. 12), and different experimental survival yields (Fig. 8). For p-OCH_3 BzPy (Figure 13B), the effective temperature evolution with the fluence differs slightly from the other two for DHB and SA, but have the same order of magnitude. It is noticeable that the ion effective temperatures found in AP-MALDI are lower than in vacuum-MALDI (see reference 38, and in the introduction). The ion effective temperature depends strongly on the matrix. In all cases, the effective temperatures are found to increase more rapidly with laser fluence for CHCA than for the other matrices, which is compatible

with the so-called “hot” character of this matrix. However, compared to the usual trend in metastable decay, SA is found to be softer than DHB in all cases. Interestingly, with the benzylpyridinium ions, the relative hardness of the matrix (CHCA > DHB > SA) correlates well with the matrix sublimation temperature (455 K > 443 K > 426 K[37]). It is also surprising that, in Figure 13A, the effective temperature first decreases with laser fluence, then increases again in the cases of DHB and SA. To date we could not find any satisfactory explanation for this observation. The fact that the evolution of the effective temperature with the laser fluence varies with the nature of the molecule calls for further studies with other classes of probe molecules.

Conclusion

In summary, in the present study of the fragmentation of benzylpyridinium ions in delayed extraction MALDI-TOF and AP-MALDI, we tried to shed a light on the different contributions to internal energy build-up in MALDI. Using benzylpyridinium as probe ions, we distinguished the following contributions:

(1) Unimolecular fragmentation (Scheme 1) in the source occurring promptly after laser irradiation (time scale < 100 ns) results either from direct energy transfer from the laser, or from matrix-to-analyte energy transfer. It translates into a sharp fragment peak visible in delayed extraction linear- or reflector-TOF. The measurement of the survival yields in AP-MALDI for several benzylpyridinium ions shows that all analytes behave like if they had the same temperature, rather than the same total internal energy. The matrix for which the highest effective temperature is obtained at high laser fluences is CHCA (T_{eff} around 1100 K). With DHB and SA, the effective temperature increases less steeply with the fluence, and SA is found softer than DHB. Lower sublimation temperature matrices seem to give lower analyte effective temperatures, but this trend is to be confirmed by further experiments with other analytes and matrices.

(2) Hydrogen radical-induced fragmentation (Scheme 2) promptly after laser irradiation also occurs shortly after laser irradiation, and results from hydrogen radical transfer from the matrix. In the benzylpyridinium ions, it results into a sharp PyH^+ peak. This process is to be correlated with the in-source decay process observed for peptides and proteins. The matrix which is most prone to these hydrogen radical reactions is DHB.

(3) In vacuum-MALDI, unimolecular fragmentation resulting from collisions between the analyte and the plume occurs 10 to 100 ns after extraction starts. This extraction-induced fragmentation is responsible for a broad delayed fragment ion peak. The proportion of “delayed” fragments compared to the “prompt” ones depends on the matrix, on the laser intensity, and, in the case of CHCA, on the extraction delay time. Extraction-induced collisional activation render the determination of the ion effective temperatures in vacuum-MALDI-TOF difficult for two reasons. First, the high spot-to-spot variability causes large standard deviations in the measurement of the ion survival yields. Second, this

fragmentation may result from very fast energy transfer upon collision of the analyte with neutral matrix molecules of the plume. In that case, the fragmentation kinetics can not be modeled using the RRKM theory.

It is likely that the observation of a delayed fragment peak is possible only in the case of small analytes only, when the collision partner in the plume – the matrix – is large compared to the analyte. In the case of larger analytes, the fragmentation will still be very efficient, but will result in metastable decay (PSD or neutral losses detectable in the reflectron mode). However the use of small probe ions like the benzylpyridinium ions is an interesting approach for investigating the extraction-induced fragmentation, and therefore the processes at the origin of metastable decay. In contrast, the prompt fragmentation is the most interesting process to gain additional information on the heart of the MALDI process, namely how the laser energy is transferred to the analyte and partitioned between kinetic energy and internal energy. AP-MALDI appears to be the method of choice for these investigations because (i) the extraction-induced fragmentation is absent, and (ii) the measurement of the survival yields is much more reproducible than in standard MALDI-TOF. Other analytes and a larger set of matrices are currently under investigation in our laboratory.

Acknowledgements

We would like to thank Agilent Technologies (Waldbronn, Germany) for the loan of the AP-MALDI 1100 series LC/MSD trap SL, and Dr. F. Mandel for technical support. VG is grateful to the FNRS (Fonds National de la Recherche Scientifique, Belgium) for a postdoctoral research fellowship and to the Alexander von Humboldt foundation for sponsoring a research stay in Germany.

Table 1. Influence of the value of *G* on the kinetics of fragmentation of p-CH_3 BzPy. Δt_{tot} = difference in flight time between the sharp and the broad peak. t_A = time elapsed between extraction and fragmentation. x_f = distance covered between extraction and fragmentation.

G	Δt_{tot} (ns)	t_A (ns)	x_f (mm)
0.96	30	59	0.32
0.94	20	35	0.17
0.92	16	25	0.12
0.90	13	19	0.086

Table 2. Summary of the different contributions to internal energy build-up in the case of the benzylpyridinium ions.

	Energy input		**Fragmentation of BzPy**	
	Origin	**When**	**Where**	**When**
1	Energy transfer from the laser, mediated by the matrix	Starts with laser impact	In the source	≤ 100 ns after laser impact
2	Reaction with hydrogen radicals in the plume	Starts with laser impact	In the source	≤ 100 ns after laser impact
3	Collisions with the neutrals of the plume	Starts with extraction	In the source	10-100 ns after extraction starts (see Figure 10C)

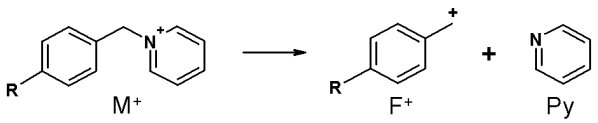

Scheme 1

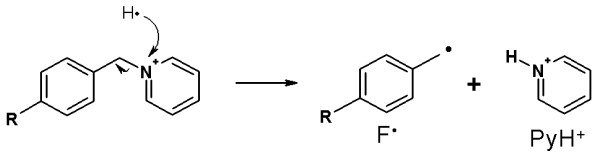

Scheme 2

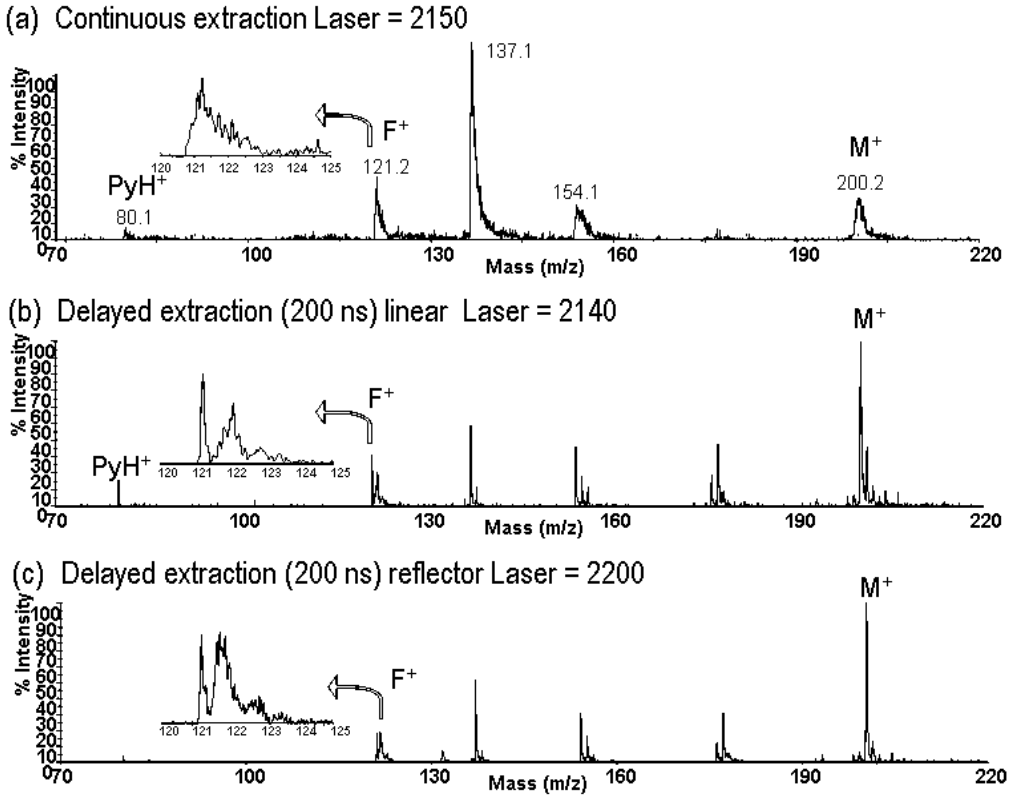

Figure 1. Typical MALDI-TOF mass spectra of p-OCH_3 benzylpyridinium in DHB (dried droplet preparation; irradiation on outer rim) in (a) continuous extraction linear mode, (b) delayed extraction (200 ns) linear mode and (c) delayed extraction (200 ns) reflector mode. The peaks around 137, 154 and 177 Th are matrix-related peaks. The insets show zooms on the benzyl fragment (theoretical nominal mass: 121 Da). U = 20 kV and G = 0.96.

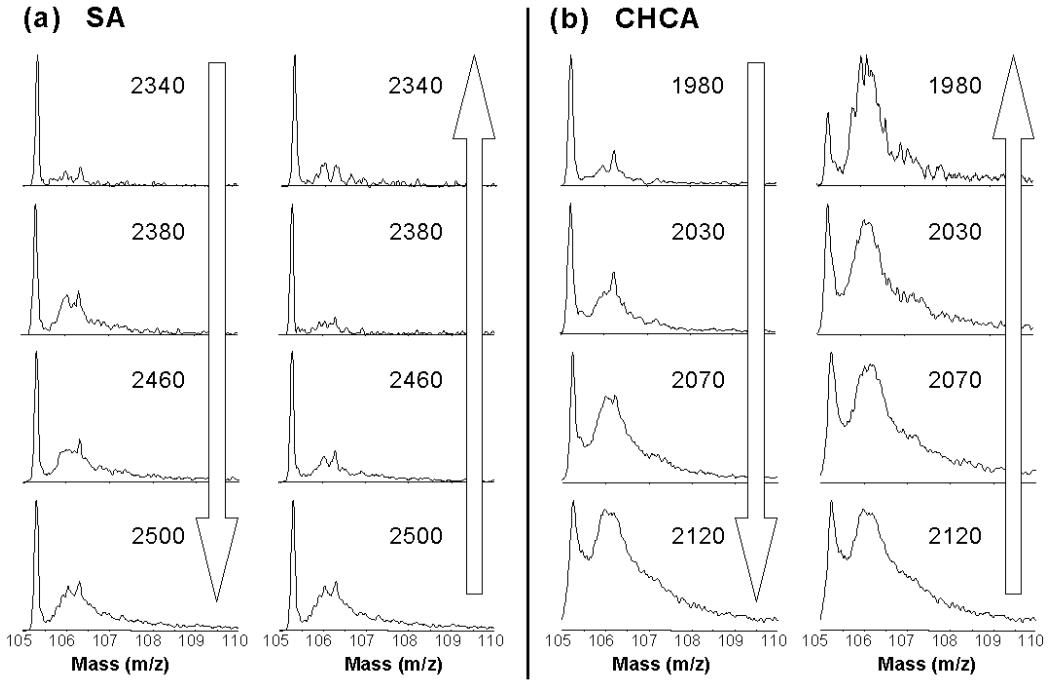

Figure 2. Influence of the laser exposure on the delayed extraction (200 ns) linear MALDI-TOF spectra of p-CH_3 benzylpyridinium in (a) sinapinic acid and (b) α-cyano-4-hydroxycinnamic acid. The spectra are the sum of 256 scans acquired by scanning the same area of the dried droplet spot. Laser intensity is first increased, then decreased. U = 20 kV and G = 0.96.

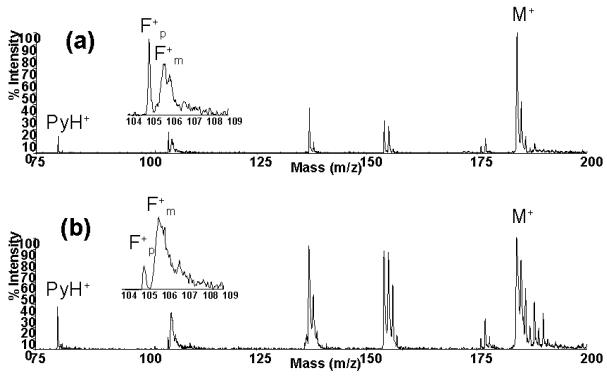

Figure 3. Influence of the laser exposure on the delayed extraction (200 ns) linear MALDI-TOF spectra of p-CH_3 benzylpyridinium in DHB (dried droplet; large crystals). (a) first spectrum acquires at a laser intensity of 2200 a.u. (threshold). (b) spectrum acquired on the same spot (but possibly other crystals) at laser intensity of 2200 after about 50 other measurements at higher laser intensities. The insets show zooms on the benzyl fragment (theoretical nominal mass: 105 Da). U = 20 kV and G = 0.96.

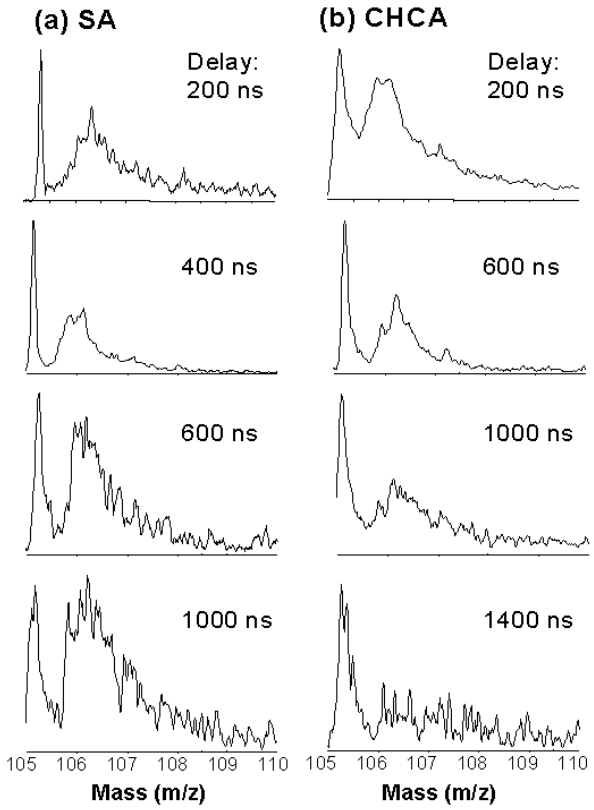

Figure 4. Influence of the delay time on the shape of the p-CH_3 benzyl fragment peak in (a) sinapinic acid at a laser intensity of 2520 and (b) α-cyano-4-hydroxycinnamic acid at a laser intensity of 2120. The spectra are the sum of 256 scans acquired by scanning the same area of the dried droplet spot. U = 20 kV and G = 0.96.

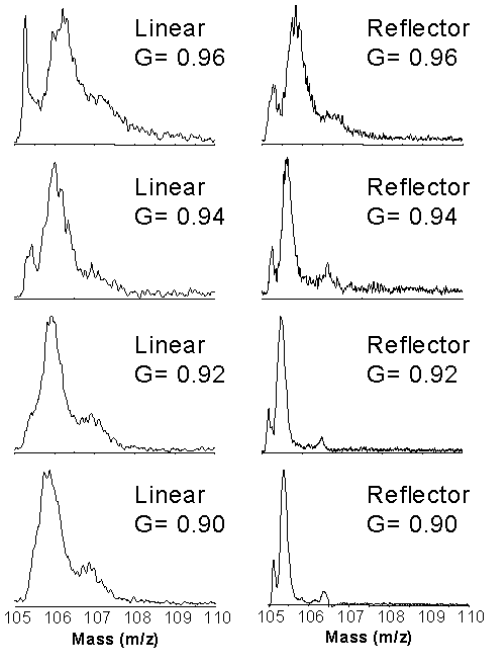

Figure 5. Influence of the value of G on the shape of the p-CH_3 benzyl fragment peak in α-cyano-4-hydroxycinnamic acid at a laser intensity of 2070. The spectra are the sum of 256 scans acquired by scanning the same area of the dried droplet spot. Left: linear mode. Right: reflector mode. U = 20 kV and extraction delay = 200 ns. The shoulder on the broad delayed peak is the ^{13}C isotope contribution.

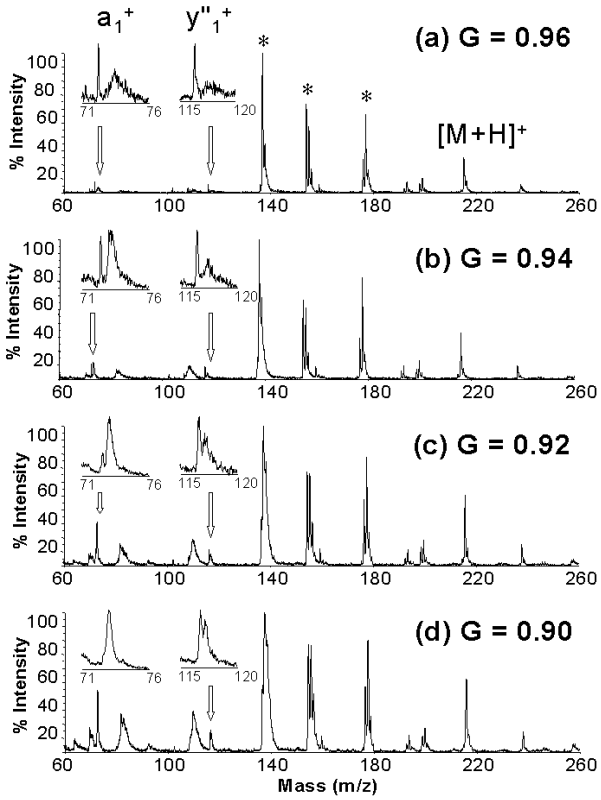

Figure 6. Delayed extraction (200 ns) linear MALDI-TOF spectra of the peptide Val-Pro ($M+H^+$ nominal mass: 215 Da) in DHB (dried droplet; large crystals) at a laser intensity of 2350 (arb. units). Influence of the value of G on the shape of the fragments $y"_1{}^+$ (theoretical nominal mass: 116 Da) and $a_1{}^+$ (72 Da). The stars denote matrix-related peaks.

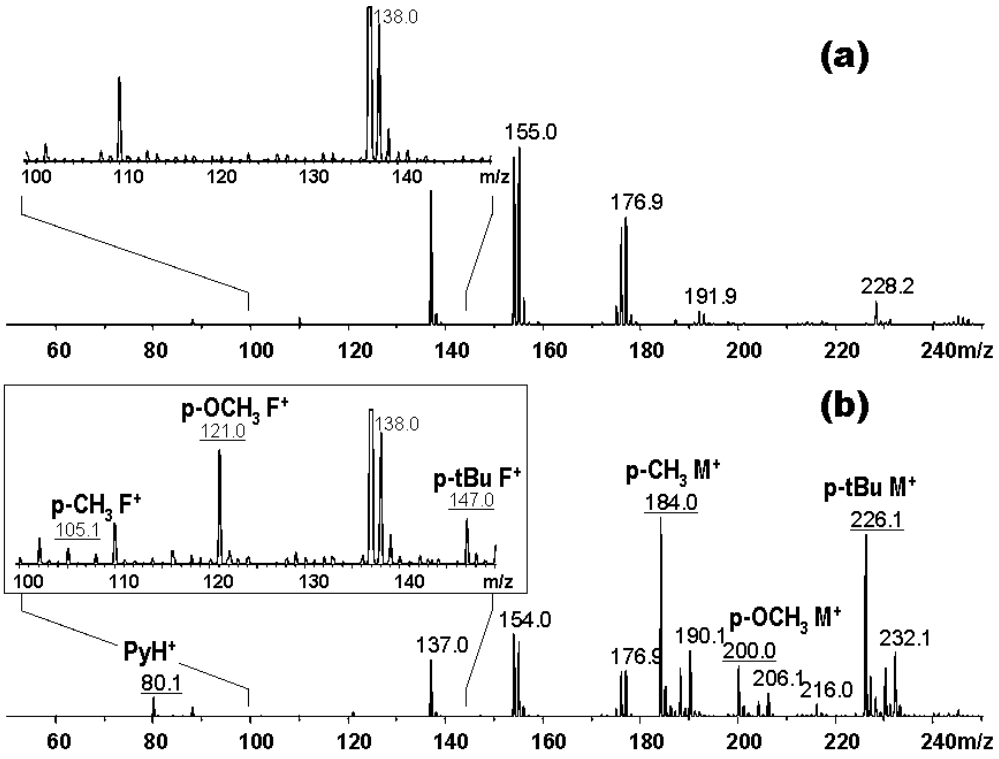

Figure 7. Representative AP-MALDI spectra, obtained with DHB at a laser fluence of 47.4 mJ/cm², with a zoom on the fragment ion region. (a) Spectrum of the matrix alone. (b) Spectrum obtained with an equimolar mixture of the three benzylpyridinium cations p-CH_3, p-OCH_3 and p-tBu. The parent ions are noted M^+ and the benzyl fragment ions are noted F^+, according to Scheme 1.

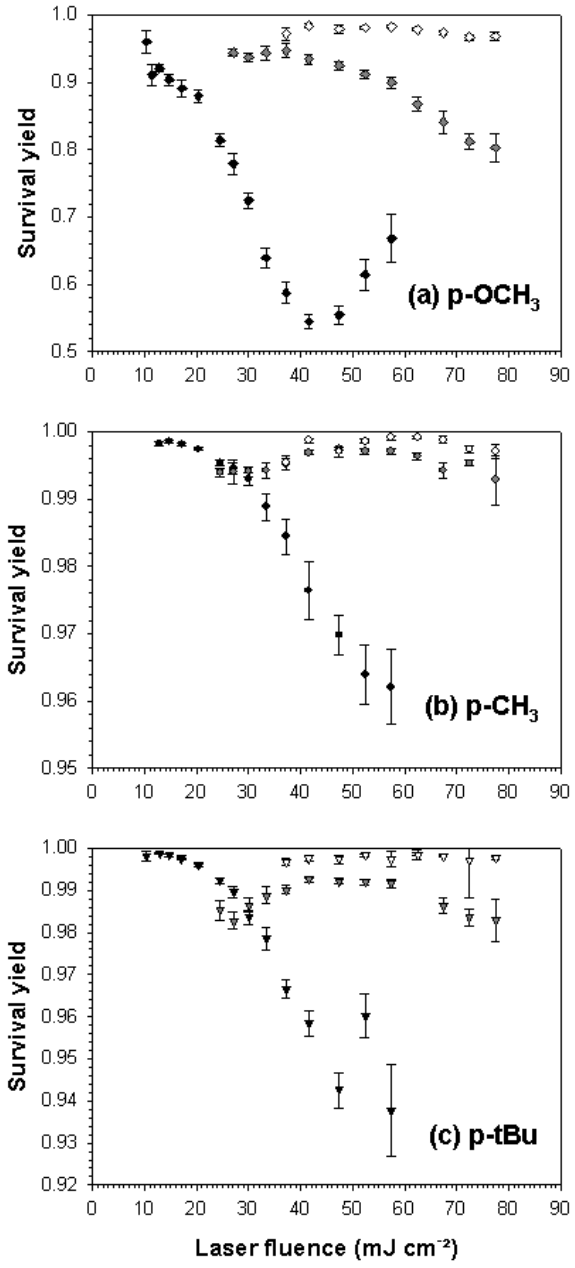

Figure 8. The survival yields of benzylpyridinium ions as a function of the laser fluence for three different matrices : CHCA (black), DHB (gray) and SA (white).

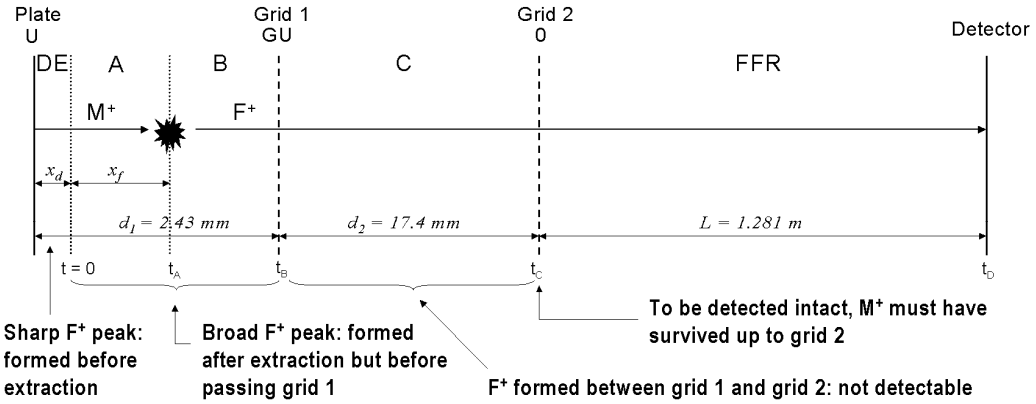

Figure 9. Scheme of the Voyager DE-PRO instrument, and model used to relate the place where fragments form to their flight time. x_d = distance covered before extraction; x_f = distance covered by the parent ion M^+ between extraction and its fragmentation into F^+; t_A = time elapsed between extraction and fragmentation of M^+.

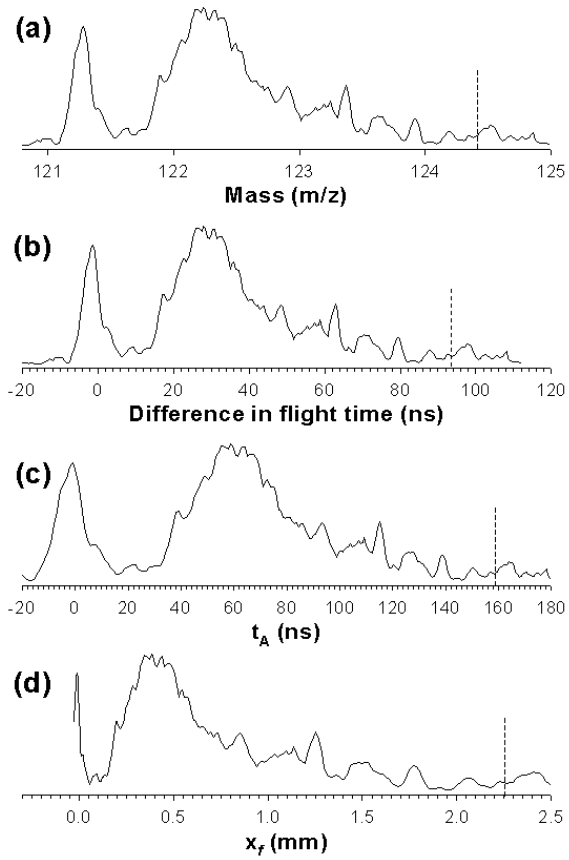

Figure 10. Conversion of the mass spectrum of p-OCH_3 benzylpyridinium (a) into the difference in flight times between the regular sharp fragment peak (b). The time where fragments from t_A (c) and the place where fragments form x_f (d) are calculated from the difference in flight times as explained in the text. Matrix: DHB dried droplet large crystals, extraction delay: 600 ns. Laser intensity: 2220 (arb. units). U = 20 kV; G = 0.96. The initial velocity is assumed to be v_0 = 400 m/s, giving x_d = 0.24 mm. The vertical dashed line shows the limit where the parent ions pass grid 1 ($x_d + x_f = d_1$).

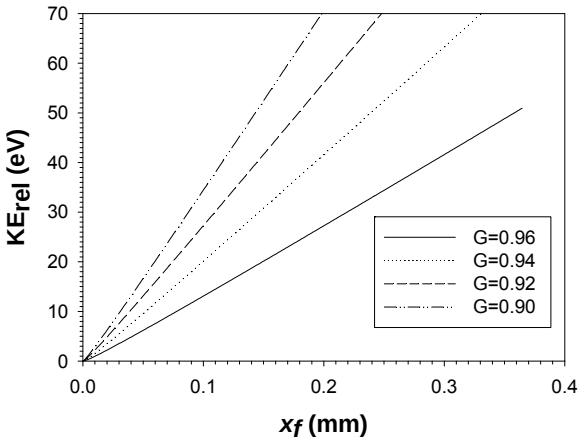

Figure 11. Relative collision energy as a function of the distance x_f (see Figure 9). Calculated using Equation (7); m_M = 200 Da (p-OCH_3 BzPy); m_{matrix} = 154 Da (DHB); v_0 = 400 m/s; v_{lab} given by the kinematic model described in Fig. 9.

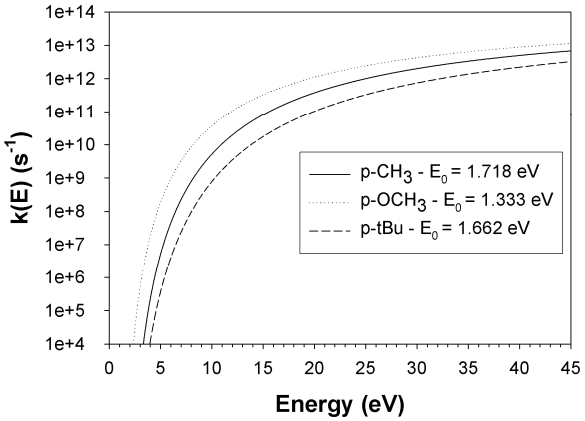

Figure 12. Unimolecular dissociation rate constants as a function of the internal energy E, calculated using the RRKM equation.

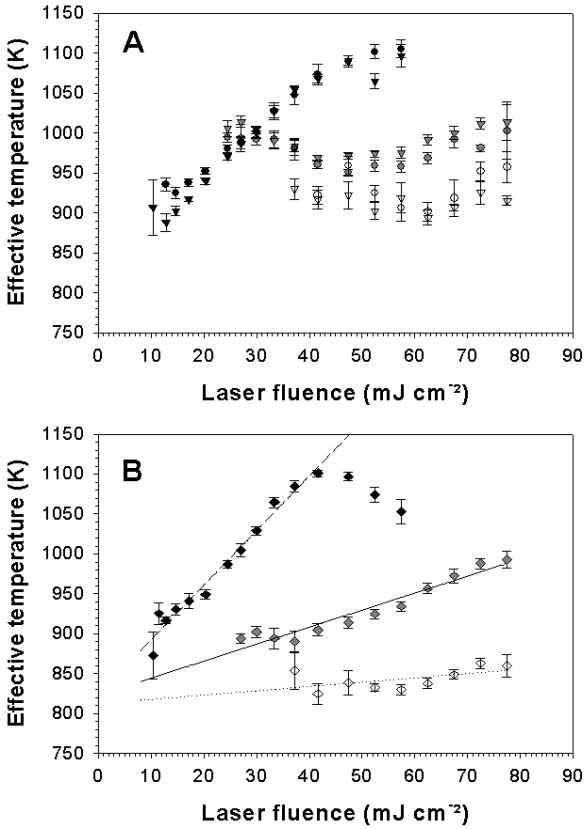

Figure 13. Effective ion temperatures (assuming a reaction time of 100 ns) in AP-MALDI. (A) p-CH_3 (circles) and p-tBu (triangles down). (B) p-OCH_3 (diamonds). Black: CHCA; gray: DHB; white: SA.

Reference List

1. Dreisewerd K. The desorption process in MALDI. *Chem. Rev.* 2003; **103**: 395-425.

2. Karas M, Krüger R. Ion formation in MALDI: the cluster ionization mechanism. *Chem. Rev.* 2003; **103**: 427-439.

3. Knochenmuss R, Zenobi R. MALDI ionization: the role of in-plume processes. *Chem. Rev.* 2003; **103**: 441-452.

4. Zhigilei LV, Leveugle E, Garrison BJ, Yingling YG, Zeifman MI. Computer simulations of laser ablation of molecular solids. *Chem. Rev.* 2003; **103**: 321-347.

5. Karas M, Bachmann D, Bahr U, Hillenkamp F. Matrix-assisted ultraviolet laser desorption of non-volatile compounds. *Int. J. Mass Spectrom. Ion. Proc.* 1987; **78**: 53-68.

6. Karas M, Hillenkamp F. Laser desorption ionization of proteins with molecular masses exceeding 10 000 Daltons. *Anal. Chem.* 1988; **60**: 2299-2301.

7. Karas M, Bahr U, Giebmann U. Matrix-assisted laser desorption mass spectrometry. *Mass Spectrom. Rev.* 1991; **10**: 335-357.

8. Hillenkamp F, Karas M, Beavis RC, Chait BT. Matrix-assisted laser desorption/ionization mass spectrometry of biopolymers. *Anal. Chem.* 1991; **63**: 1193 A-1202 A.

9. Zhu L, Parr GR, Fitzgerald MC, Nelson CM, Smith LM. Oligodeoxynucleotide fragmentation in MALDI/TOF mass spectrometry using 355-nm radiation. *J. Am. Chem. Soc.* 1995; **117**: 6048-6056.

10. Simmons TA, Limbach PA. Influence of co-matrix proton affinity on oligonucleotide ion stability in MALDI TOF MS. *J. Am. Soc. Mass Spectrom.* 1998; **9**: 668-675.

11. Gross J, Leisner A, Hillenkamp F, Hahner S, Karas M, Schäfer J, Lützenkirchen F, Nordhoff E. Investigations of the metastable decay of DNA under UV - MALDI conditions with postsource decay analysis and H/D exchange. *J. Am. Soc. Mass Spectrom.* 1998; **9**: 866-878.

12. Gross J, Hillenkamp F, Wan KX, Gross ML. Metastable decay of negatively charged oligodeoxynucleotides analyzed with ultraviolet matrix-assisted laser desorption/ionization post-source decay and deuterium exchange. *J. Am. Soc. Mass Spectrom.* 2001; **12**: 180-192.

13. Schnölzer M, Lehmann WD. Identification of modified peptides by meatastable fragmentation in MALDI mass spectrometry. *Int. J. Mass Spectrom. Ion. Proc.* 1997; **169/170**: 263-271.

14. Annan RS, Carr SA. Phosphopeptide analysis my matrix-assisted laser desorption time-of-flight mass spectrometry. *Anal. Chem.* 1996; **68**: 3413-3421.

15. Karas M, Bahr U, Strupat K, Hillenkamp F, Tsarbopopoulos A, Paamanik BN. Matrix dependance of metastable fragmentation of glycoproteins in MALDI TOF mass spectrometry. *Anal. Chem.* 1995; **67**: 675-679.

16. Karas M, Bahr U, Stahl-Zheng J-R. Steps towards a more refined picture of the matrix function in UV MALDI.In: *Large ions: their vaporization, detection and structural analysis* eds Baer T, Ng CY, Powis I, John Wiley and Sons, 1996: 27-48.

17. Spengler B, Kirsch D, Kaufmann R. Metastable decay of peptides and proteins in matrix-assisted laser-desorption mass spectrometry. *Rapid Commun. Mass Spectrom.* 1991; **5**: 198-202.

18. Spengler B, Kirsch D, Kaufmann R. Fundamental aspects of postsource decay in MALDI mass spectrometry. *J. Phys. Chem.* 1992; **96**: 9678-9684.

19. Spengler B. Postsource decay analysis in matrix-assisted laser desorption/ionization mass spectrometry of biomolecules. *J. Mass Spectrom.* 1997; **32**: 1019-1036.

20. Szilagi Z, Varney JE, Derrick PJ. Dependance of MALDI - PSD spectra on laser power. *Rapid Commun. Mass Spectrom.* 1998; **12**: 489-492.

21. Bökelmann V, Spengler B, Kaufmann R. Dynamical parameters of ion ejection and ion formation in MALDI. *Eur. Mass Spectrom.* 1995; **1**: 81-93.

22. Patterson SD, Katta V. Prompt fragmentation of disulfide-linked peptides during matrix-assisted laser desorption/ionization mass spectrometry. *Anal. Chem.* 1994; **66**: 3727-3732.

23. Brown RS, Lennon JL. Sequence-specific fragmentation of matrix-assisted laser-desorbed protein/peptide ions. *Anal. Chem.* 1995; **67**: 3990-3999.

24. Brown RS, Carr BL, Lennon JL. Factors that influence the observed fast fragmentation of peptides in matrix-assisted laser desorption. *J. Am. Soc. Mass Spectrom.* 1996; **7**: 225-232.

25. Brown RS, Feng J, Reiber DC. Further studies of in-source fragmentation of peptides in MALDI. *Int. J. Mass Spectrom. Ion. Proc.* 1997; **169/170**: 1-18.

26. Katta V, Chow DT, Rohde MF. Applications of in-source fragmentation of protein ions for direct sequence analysis by delayed extraction MALDI-TOF mass spectrometry. *Anal. Chem.* 1998; **70**: 4410-4416.

27. Reiber DC, Grover TA, Brown RS. Identifying proteins using MALDI in-source fragmentation data combined with database searching. *Anal. Chem.* 1998; **70**: 673-683.

28. Reiber DC, Brown RS, Weinberger S, Kenny J, Bailey J. Unknown peptide sequencing using MALDI and in-source decay. *Anal. Chem.* 1998; **70**: 1214-1222.

29. Takayama M, Tsugita A. Sequence information of peptides and proteins with in-source decay in matrix assisted laser desorption/ionization-time of flighe-mass spectrometry. *Electrophoresis* 2000; **21**: 1670-1677.

30. Takayama M. N-C_α bond cleavage of the peptide backbone via hydrogen abstraction. *J. Am. Soc. Mass Spectrom.* 2001; **12**: 1044-1049.

31. Takayama M. In-source decay characteristics of peptides in MALDI TOF mass spectrometry. *J. Am. Soc. Mass Spectrom.* 2001; **12**: 420-427.

32. Koomen JM, Russell D. Ultraviolet/matrix-assisted laser desorption/ionization mass spectrometric characterization of 2,5-dihydroxybenzoic acid-induced reductive hydrogenation of oligonucleotides on cytosine residues. *J. Mass Spectrom.* 2000; **35**: 1025-1034.

33. Zubarev RA, Haselmann KF, Budnik BA, Kjeldsen F, Jensen F. Towards an understanding of the mechanism of eletron-capture dissociation: a historical perspective and modern ideas. *Eur. Mass Spectrom.* 2002; **8**: ?

34. Scott CTJ, Kosmidis C, Jia WJ, Ledingham KWD, Singhal RP. Formation of atimic hydrogen in matrix-assisted laser desorption ionisation. *Rapid Commun. Mass Spectrom.* 1994; **8**: 829-832.

35. Huth-Fehre T, Becker CH. Energetics of gramicidin S after UV laser desorption from a ferulic acid matrix. *Rapid Commun. Mass Spectrom.* 1991; **5**: 378-382.

36. Mowry CD, Johnston MV. Internal energy of neutral molecules ejected by matrix-assisted laser desorption. *J. Phys. Chem.* 1994; **98**: 1904-1909.

37. Stevenson E, Breuker K, Zenobi R. Internal energies of analyte ions generated from different MALDI matrices. *J. Mass Spectrom.* 2000; **35**: 1035-1041.

38. Luo G, Marginean I, Vertes A. Internal energy of ions generated by matrix-assisted laser Desorption/Ionization. *Anal. Chem.* 2002; **74**: 6185-6190.

39. Collette C, De Pauw E. Calibration of the internal energy distribution of ions produced by electrospray. *Rapid Commun. Mass Spectrom.* 1998; **12**: 165-170.

40. Collette C, Drahos L, De Pauw E, Vékey K. Comparison of the internal energy distributions of ions produced by different electrospray sources. *Rapid Commun. Mass Spectrom.* 1998; **12**: 1673-1678.

41. Drahos L, Heeren RMA, Collette C, De Pauw E, Vékey K. Thermal energy distributions observed in electrospray ionization. *J. Mass Spectrom.* 1999; **34**: 1373-1379.

42. Greisch J-F, Gabelica V, Remacle F, De Pauw E. Thermometer ions for matrix-enhanced laser desorption/ionization internal energy calibration. *Rapid Commun. Mass Spectrom.* 2003; **17**: 1847-1854.

43. Vertes A, Levine RD. Sublimation vs fragmentation in matrix-assisted laser desorption. *Chem. Phys. Lett.* 1990; **171**: 284-290.

44. Vertes A, Gijbels R, Levine RD. Homogeneous bottleneck model of matrix-assisted ultraviolet laser desorption of large molecules. *Rapid Commun. Mass Spectrom.* 1990; **4**: 228-233.

45. Vertes A, Irinyi G, Gijbels R. Hydrodynamic model of matrix-assisted laser desorption mass spectrometry. *Anal. Chem.* 1993; **65**: 2389-2393.

46. Glückmann M, Karas M. The initial velocity and its dependence on matrix, analyte and preparation method in ultraviolet matrix-assisted laser desorption/ionization. *J. Mass Spectrom.* 1999; **34**: 467-477.

47. Dreisewerd K, Schürenberg M, Karas M, Hillenkamp F. Influence of laser intensity and spot size on the desorption of molecules and ions in MALDI with a uniform beam profile. *Int. J. Mass Spectrom. Ion. Proc.* 1995; **141**: 127-148.

48. Knochenmuss R. A quantitative model of ultraviiolet matrix-assisted laser desorption/ionization. *J. Mass Spectrom.* 2002; **37**: 867-877.

49. Bencsura A, Navale V, Sadeghi M, Vertes A. Matrix-guest energy transfer in MALDI. *Rapid Commun. Mass Spectrom.* 1997; **11**: 679-682.

50. Zeifman MI, Garrison BJ, Zhigilei LV. Combined molecular dynamics-direct simulation Monte Carlo computational study of laser ablation plume evolution. *J. Appl. Phys.* 2002; **92**: 2181-2193.

51. Zhigilei LV. Dynamics of the plume formation and parameters of the ejected clusters in short-pulse laser ablation. *Appl. Phys. A* 2003; **76**: 339-350.

52. De Pauw E, Pelzer G, Marien J, Natalis P. Internal energy distribution of ions emitted in secondary ion mass spectrometry. *Org. Mass Spectrom.* 1990; **25**: 103-108.

53. Derwa F, De Pauw E, Natalis P. New basis for a method for the estimation of secondary ion internal energy distribution in "soft" ionisation techniques. *Org. Mass Spectrom.* 1991; **26**: 117-118.

54. Scott AP, Radom L. Harmonic vibrational frequencies: an evaluation of Hartree-Fock, Moller-Plesset, quadratic configuration interaction, density functional theory, and semiempirical scale factors. *J. Phys. Chem.* 1996; **100**: 16502-16513.

55. Dunbar RC. New approaches to ion thermochemistry via dissociation and association. *Adv. Gas Phase Ion Chem.* 1996; **2**: 87-124.

56. Speir JP, Amster IJ. An investigation of the energetics of peptide ion dissociation by laser desorption chemical ionization fourier transform mass spectrometry. *J. Am. Soc. Mass Spectrom.* 1995; **6**: 1069-1078.

57. Kinsel GR, Edmondson RD, Russell DH. Profile and flight time analysis of bovine insulin clusters as a probe of MALDI ion formation dynamics. *J. Mass Spectrom.* 1997; **32**: 714-722.

58. Meroueh SO, Wang YF, Hase WL. Direct dynamics Simulations of collision- and surface-induced dissociation of N-protonated glycine. Shattering fragmentation. *J. Phys. Chem. A* 2002; **106**: 9983-9992.

59. Laskin J, Bailey TH, Futrell JH. Shattering of peptide ions on self-assembles monolayer surfaces. *J. Am. Chem. Soc.* 2003; **125**: 1625-1632.

60. Vékey K. Internal energy effects in mass spectrometry. *J. Mass Spectrom.* 1996; **31**: 445-463.

61. Drahos L, Vékey K. How closely related are the effective and the real temperature. *J. Mass Spectrom.* 1999; **34**: 79-84.